Journal of Magnetism and Magnetic Materials 587 (2023) 171275

Contents lists available at ScienceDirect

Journal of Magnetism and Magnetic Materials

journal homepage: www.elsevier.com/locate/jmmm

In vitro evaluation of magnetic fluid hyperthermia therapy on breast cancer cells using monodispersed $Mn_{0.5}Zn_{0.5}Fe_2O_4$ nanoflowers

Hima Patel [a,b], Kinnari Parekh [a,b,*], Lionel Fernel Gamarra [c], Javier Bustamante Mamani [c], Arielly da Hora Alves [c], A.M. Figueiredo Neto [d]

[a] Dr. K C Patel R & D Centre, Charotar University of Science and Technology, CHARUSAT Campus, Changa 388421, Gujarat, India
[b] P D Patel Institue of Applied Sciences, Charotar University of Science and Technology, CHARUSAT Campus, Changa 388421, Gujarat, India
[c] Hospital Israelita Albert Einstein, Av. Albert Einstein 627/701, Morumbi, São Paulo, Brazil
[d] Instituto de Física, Universidade de São Paulo, P.O. Box 66318, São Paulo 05389-970, SP, Brazil

ARTICLE INFO

Keywords:
Nanoflowers
Magnetic properties
Magnetic fluid hyperthermia
Breast cancer cells

ABSTRACT

Magnetic fluid hyperthermia (MFH) is emerging as an alternate treatment therapy for cancer of different types, due to its potential low side effects and relatively less painless treatment option. However, the implementation of standalone therapy is still challenging and needs research to optimize the effective killing of 100% cancerous tissues, number of therapy sessions, time duration of the therapy, controlled hyperthermia window temperature, etc. We report here the potential of nanoclusters (nanoflowers) based dispersion and on an *in vitro* study on breast cancer cells (MDA-MB-231). The nanoclusters were characterized using XRD, TEM, DLS, VSM and MFH, before investigating them with breast cancer cells. The effect of MFH, before and after the treatment of induction heating on MDA-MB-231 cells, were also studied. Results show that the MFH is capable of killing almost 87% of cells within 30 min of treatment on cells in the presence of magnetic nanoclusters. This shows the potential of developing nanoflowers for the treatment of cancer over other single domain magnetic nanoparticles.

1. Introduction

Magnetic fluid hyperthermia (MFH) is emerging as a potential therapy method for cancers of different types [1]. In the MFH, the heat will be generated by the magnetic nanoparticles via magnetic energy loss in the presence of an external alternating magnetic field [2,3]. The heating ability of magnetic nanoparticles depends on the specific absorption rate (SAR) and it's a function of composition, size, shape, size distribution and magnetic properties of the materials [4]. Since the heating is achieved from the response of particles towards the applied AC magnetic field, it is possible to manipulate the heat by manipulating the magnetic response of the particles. To maintain the hyperthermia window temperature and prevent from the overheating, it is proposed to use low Curie temperature magnetic nanoparticles (MNPs). The low curie temperature of MNPs will automatically stop heating once it reaches the Curie temperature and it will work as a temperature control magnetic switch. For MFH, a range of magnetic materials like magnetite, maghemite and pure metal-based nanoparticles dispersion are employed [5,6]. Pure metals being toxic, their use for biomedical application is restricted. The iron oxide nanoparticles, due to its high Curie temperature, pose a limitation to control the hyperthermia window temperature of 315–319 K in spite of having a good biocompatibility [7–10]. In recent times, several temperature sensitive magnetic fluids doped with different metals in iron oxide nanoparticles were reported, such as $M_xFe_{1-x}Fe_2O_4$ (M = Mn, Zn, Co, Ni, Cu, etc.) [11,12], $M_xFe_{1-x}Fe_{2-y}A_yO_4$ (A = Gd, Ho, Sm, Li, etc.) [13,14] and $La_xSr_{1-x}MnO_3$ [15]. Among these materials, the Mn-Zn ferrite based MNPs have more potential due to its capacity to tune the Curie temperature and yet maintain the biocompatibility and high magnetic response at room temperature [16,17]. Especially in Mn-Zn ferrites, $Mn_{0.5}Zn_{0.5}Fe_2O_4$ composition has a low Curie temperature of ~340 K, moderately high saturation magnetization of ~210 kA/m at room temperature and high pyromagnetic coefficient (~5 kA/m•K) [18]. Due to these properties, it is possible to maintain the hyperthermia window temperature during the treatment session without altering the applicator parameters and without damaging the healthy tissues.

The study reported that biomedical application in MFH using monodispersed magnetic nanoclusters were limited to iron oxides. Ganesan

* Corresponding author.
E-mail address: kinnariparekh.rnd@charusat.ac.in (K. Parekh).

https://doi.org/10.1016/j.jmmm.2023.171275
Received 6 August 2023; Received in revised form 13 September 2023; Accepted 17 September 2023
Available online 18 September 2023

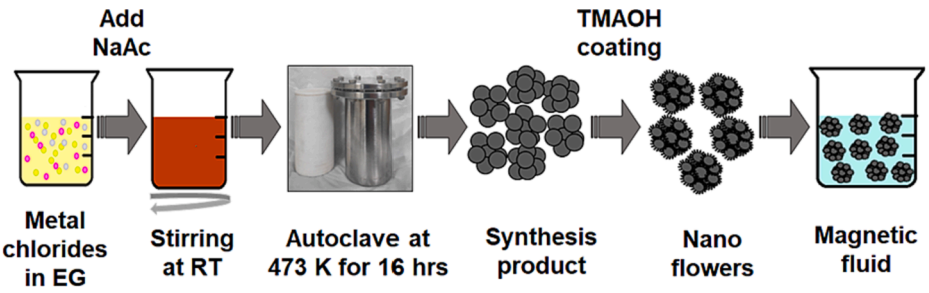

Fig. 1. Schematic of synthesis of nanoflowers based magnetic fluid.

et al. [19] reported the MFH response of poly acrylic acid (PAA) coated monodispersed magnetic nanoclusters at a frequency of 126 kHz and the magnetic field varied from 20.2 kA/m to 31.6 kA/m for two sizes 640 nm and 455 nm and the maximum SAR value of ~ 80.5 W/g. Moreover, the chitosan and dextran coated magnetic nanocrystals (MNCs) hyperthermia response reported by Jamir et al. [20] for 336 kHz frequency and 14.92 kA/m magnetic field strength for different concentration of 1 – 3 mg/mL. The cytotoxicity of both the fluid performed by an MTT assay on MG-63 cells and it resulted in to more than 90% of viability up to 1 mg/mL concentration. Similarly, the *in vitro* study of MNCs on B16-F10 (melanoma cells- skin cancer) and A549 cells under the AC magnetic field of 37.4 kA/m and frequency of 500 kHz with 1.0 mg/mL of fluid concentration for 10 min resulted in the negligible toxic effect on the cells, whereas Co doped MNCs showed the high toxicity even at low concentration [21]. However, there is no study reported for *in vitro* MFH using Mn-Zn ferrites nanoflowers based magnetic fluid.

In the present study we report the synthesis of monodispersed tetramethylammonium hydroxide coated $Mn_{0.5}Zn_{0.5}Fe_2O_4$ (A55) magnetic nanoflowers based magnetic fluid. The synthesized sample was characterized by X-Ray Diffractometer (XRD), Transmission Electron Microscope (TEM), Dynamic Light Scattering (DLS), and Vibrating Sample Magnetometer (VSM) to determine the structural, morphological, and magnetic properties of nanoflowers. We also reported here the investigation of induction heating of nanoflowers on a magnetic field of 23.87 kA/m and frequency of 309 kHz, internalization and cytotoxicity test of magnetic nanoparticles based magnetic fluid on breast cancer cells (MDA-MB-231) and *in vitro* MFH effect of nanoflowers on breast cancer cell along with bioluminescence imaging (BLI) technique for observing cell death study before and after the hyperthermia treatment.

2. Experimental

2.1. Synthesis of nanoflowers

Iron (III) chloride hexahydrate ($FeCl_3{\cdot}6H_2O$(s), 98%), Manganese (II) chloride tetra hydrate ($MnCl_2{\cdot}4H_2O$(s), 98%) and tetramethylammonium hydroxide (TMAOH, $(CH_3)_4N + OH–$, ≥98%) were purchased from Sigma Aldrich. Sodium acetate tri-hydrate ($CH_3COONa{\cdot}3H_2O$, 99.5%) was purchased from Merck, Ethylene Glycol (99%) was from Samir Tech-Chem. Pvt Ltd. India and Zinc (II) chloride ($ZnCl_2$(dry), 98%) was purchased from LOBA Chemie Pvt. Ltd., India. All of these chemicals were used, without any additional purification.

The self-regulating temperature sensitive iron oxide-based monodispersed magnetic nanoflowers were synthesized using hydrothermal techniques. In the synthesis of $Mn_{0.5}Zn_{0.5}Fe_2O_4$ nanoflowers (A55HT16) the molar ratio of Mn:Zn:Fe precursor was taken as 0.5:0.5:2. The Mn^{2+}, Zn^{2+} and Fe^{3+} salts (14.8 mM) were added into 160 mL of ethylene glycol (EG) along with 0.175 M of precipitating agent sodium acetate (NaAc). The mixture was stirred at room temperature for 30 min and then transferred to a sealed Teflon lined autoclave and heated for 16 h at 473 K. The resultant product, after cooling down to room temperature, was washed with distilled water thrice. Then 1/3rd part of the synthesized sample was used for the coating using 50 mL of tetramethylammonium hydroxide (TMAOH) using one-hour sonication. The last step was repeated two times. The excess TMAOH was removed by magnetic sedimentation and the coated sample is dispersed into distilled water. The pictorial representation of the synthesis procedure is shown in Fig. 1.

2.2. Characterization by XRD, TEM, DLS, and VSM

The X-Ray Diffractometer (XRD, Bruker, D2 PHASER, Germany) attached with the Copper K_α source (wavelength = 0.15414 nm) and the Lynx-Eye detector operated at 30 kV and 10 mA was used to determine the crystal structure, phase purity, crystallite size and lattice parameter of the magnetic nanoparticles. The measurement was done between 15° to 65° angular range (2θ) with a 0.05° increment. The transmission electron microscope (TEM, JEOL JEM-2100) with LaB6 filament accelerated at 200 kV was used to measure the microscopic images of the samples. Both the parent fluid as well as its dilution were sonicated at least for 30 min before preparing the sample. A drop of a diluted fluid was placed on a collagen coated Cu grid after sonication of the diluted fluid. The grid was dried under vacuum for about 24 h. The colloidal properties of samples were investigated using dynamic light scattering (DLS, Malvern Nano S90) to determine the hydrodynamic particle size and polydispersity of particles. The sample was diluted to 0.15 mg/mL using ammoniated water. The parent fluid and its dilution were both sonicated for 10 min before the sample used for the measurement. The 1 mL of fluid was used for the characterization and the measurement was carried out at 298 K temperature. The parameters set for measurement were 1.33, the refractive index, and 1.0016 mPa•s was the viscosity of water used as a dispersant. The magnetic properties of the magnetic fluid were measured with a vibrating sample magnetometer (VSM, LakeShore Model 7404, USA), at room temperature (300 K) with the magnetic field ranging from 0 to 1.2 T. The magnetometer was calibrated using NIST approved Ni sphere prior to the measurement.

2.3. Induction heating of fluid

To determine the heating potential of the nanoparticles, 500 μL of nanoflowers at a concentration of 1.8 mg/mL were dispersed in an aqueous medium and thermally isolated in a glass container, keeping the room temperature at 293 K. The heating curves (temperature versus time) of the samples were acquired in the following configurations: magnetic field of 23.87 kA/m associated with a frequency of 309 kHz. The AMF model DM100 system (nB nanoScale Biomagnetics) was used for the induction heating of magnetic fluid as well as for *in vitro* study on MDA-MB-231 cells with the magnetic fluid. The sample's temperature was monitored by optical fiber (3204, Luxtron Corp., Santa Ana, California, USA).

2.4. MDA-MB-231 cell culture

MDA-MB-231 breast cancer tumor cells were obtained from the Rio de Janeiro Cell Bank. The cells were cultured in DMEM-F12 medium (GIBCO ® Invitrogen Corporation, CA, USA), supplemented with 10%

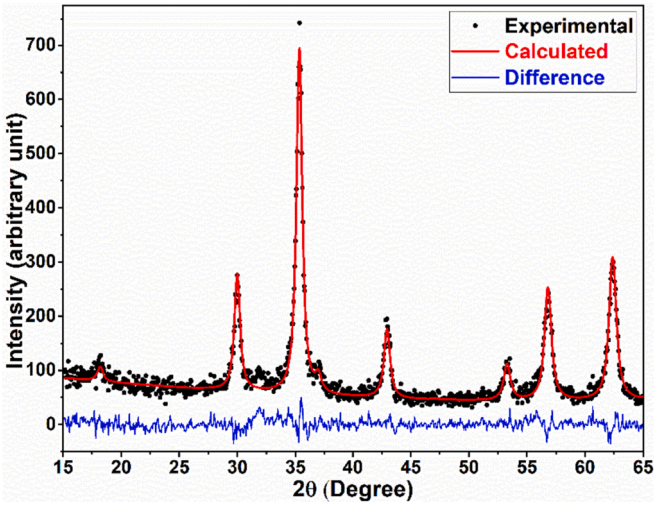

Fig. 2. XRD pattern (Scatter) of the sample A55HT16 with MAUD refined pattern (red line). (For interpretation of the references to color in this figure legend, the reader is referred to the web version of this article.)

fetal bovine serum (FBS) (GIBCO® Invitrogen Corporation, CA, USA) and incubated at 310 K (5% of CO_2) until reaching 70% confluence. They were then washed with phosphate-buffered saline solution (PBS) and tripsinized with 2 mL of 0.04% trypsin-EDTA. Subsequently, the cells were centrifuged and re-suspended in the DMEM-F12 culture medium. As the aim of evaluating the effectiveness of magnetic hyperthermia therapy, MDA-MB-231 cells were genetically modified to generate cells that express luciferase similarly to the work of Da Silva H. R. et al. [22].

2.5. Cell viability test by bioluminescence (BLI) technique

For the evaluation of viability, nanoflowers -tagged MDA-MB-231 was cultured in 96-well plates. Nanoflowers were then added to the cells at concentrations of 10, 20, 30, 40 and 50 μg/mL and incubated for 18 h. After incubation, the culture medium was discarded and 100 μL of fresh medium was added to the cells per well, after thorough washing with PBS. Subsequently, 100 μL of luciferin were added to each well and BLI images were acquired using the IVIS® Lumina LT Series III equipment for BLI intensity analysis (photons/sec). The percentage of viability was calculated using the ratio (sample/control) × 100.

2.6. Nanoflowers internalization test in breast cancer tumor cells

To evaluate the internalization of nanoflowers in MDA-MB-231 cells, the cells were plated (10^5 cells/well) in a 24-well plate and after reaching a confluence of 70%, labeling was carried out with five concentrations used (10, 20, 30, 40 and 50 μg/mL) for a period of 18 h. To evaluate the internalization, Prussian blue staining was used according to the protocol described in Nucci MP, et al. [23]. After labeling the cells, the images were recorded on a Nikon TiE microscope (Nikon, Tokyo, Japan).

2.7. In vitro evaluation of magneto hyperthermia therapy on MDA-MB-231 breast cancer cells

For the evaluation of *in vitro* MFH therapy, 3 experimental groups were delineated: MDA-MB-231, MDA-MB-231 + nanoflowers and MDA-MB-231 + nanoflowers + MFH. After labeling MDA-MB-231 with nanoflowers and analyzing internalization and viability, the best condition for applying the MFH technique was selected. For the MFH therapy process, 10^6 cells were placed in the sample holder suspended in the DMEM-F12 culture medium in the nanoflower solution. These were placed in the sample holder and MFH (23.87 kA/m; 309 kHz) was applied. The application of MFH (23.87 kA/m; 309 kHz) followed the heating schedule to maintain a constant temperature of 317 K for a period of 40 min. The bioluminescence evaluation was performed before and after the MFH process, similar to that performed in section 2.5.

3. Results and discussion

3.1. Structural characterization by XRD, TEM, DLS, zeta sizer, and magnetic measurement

Fig. 2 shows the XRD pattern (scatter) of the sample A55HT16 with the MAUD refined XRD pattern (red line). The diffraction pattern confirms the single-phase cubic spinel structure for all samples. The corresponding indexing for all the peaks in samples was (111), (220), (311), (400), (422), (511) and (440) confirming the face centered cubic (FCC) structure. There were no extra peaks found in any sample, which indicates the purity of the sample. The XRD pattern fits with an Fd-3 m space group with an inverse spinel structure. The crystallite size and the lattice parameters that were calculated from refinement were 19.2 ± 0.4 nm and 0.8419 ± 0.0002 nm, respectively. (The typical reported lattice parameter for the $Mn_{0.5}Zn_{0.5}Fe_2O_4$ bulk system is 0.8421 nm). The obtained lattice constant value of the sample is very close to the reported value of the bulk system [24].

The morphological characterization as seen from the TEM image of the sample is shown in Fig. 3(a) which shows the particles in the form of clusters as nanoflowers. Fig. 3(b) shows the HRTEM image with the atomic arrangement of the (311) plane. Fig. 3(c) shows the fast fourier transform (FFT) equidistance dot pattern. The cluster size and the standard deviation were calculated from the analysis of ~ 200 clusters using ImageJ software. The Fig. 3(d) shows the obtained distribution plot fitted with lognormal distribution function. The mean size of the cluster was 106.8 nm with a standard deviation of 0.10. Fig. 3(e) shows the single cluster of A55HT16 sample and it shows that clusters are made up of number of nanoparticles accumulated to make a nanocluster. The size and size distribution of particles within a cluster are calculated by the lognormal distribution function. The Fig. 3(f) shows the mean particle size and size distribution of the particles in a single cluster the value obtained from the fitting was 19.25 nm and the standard deviation of 0.07. The Fig. 3(g) shows the selected area energy diffraction (SAED) pattern of the sample.

The hydrodynamic size of clusters is obtained from intensity, volume, and number distribution using DLS. The results of all three; intensity, volume and number distributions for the A55HT16 sample are mentioned in Fig. 4(a) to (c), respectively. The intensity distribution is most sensitive to the cluster size as it is proportional to the 6th power of the size. Whereas the volume distribution is proportional to the 3rd power of the size. The value of hydrodynamic cluster distribution is then fitted using the lognormal distribution function. The diameter obtained from the fit is 114.2 ± 0.5 nm, 77.8 ± 0.6 nm and 54.4 ± 0.3 nm, respectively for the intensity, volume and number distribution. The DLS result shows that the hydrodynamic diameter of the cluster found from the intensity distribution is very close to the diameter obtained from the TEM images.

The magnetic response of the fluid as a function of the field is shown in Fig. 5. The magnetic characterization experiment was carried out at room temperature (300 K). The resultant curve of fluid magnetization fitted with the core shell model [25] assumes the volume distribution of particles with the log-normal probability distribution function as shown in Eq. (1).

$$M(H)f(V) = \int_0^\infty f(V) \bullet \left[M_s L(\alpha) + \chi_{pm} H\right] dV \quad (1)$$

Where, L(α) is the Langevin function, L(α) = coth (α) – 1/α. Here, α =

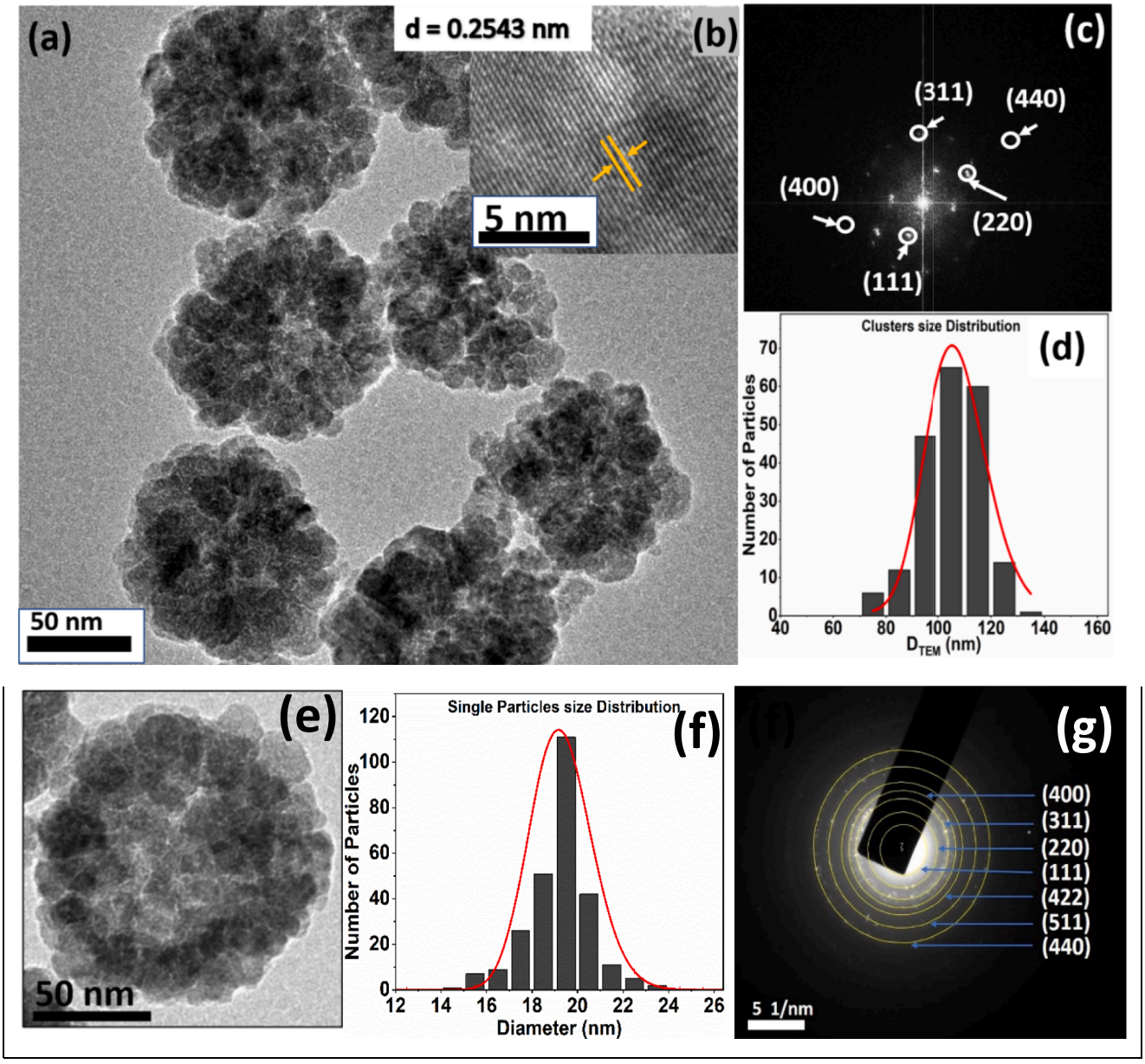

Fig. 3. (a) TEM image of the A55HT16 sample (b) HRTEM (c) FFT pattern (d) cluster distribution (e) single cluster image (f) particle size distribution in the single cluster fitted with the log normal distribution function (red line) (g) SAED pattern of the sample. (For interpretation of the references to color in this figure legend, the reader is referred to the web version of this article.)

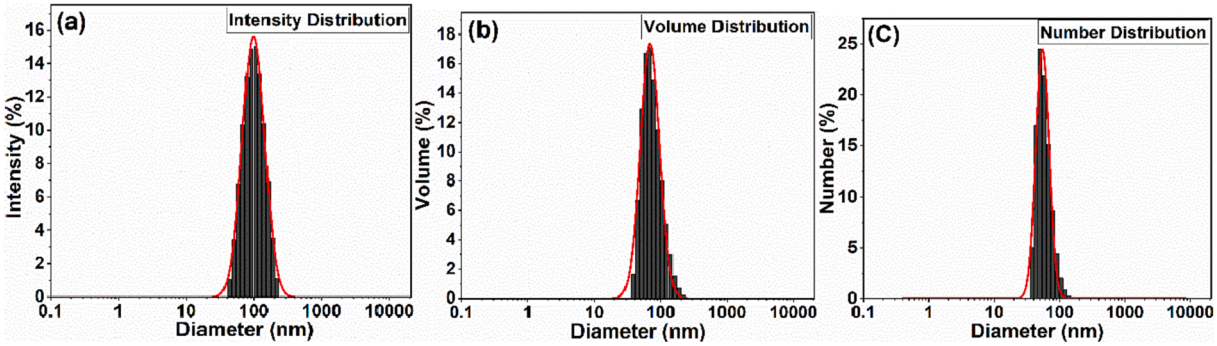

Fig. 4. DLS results of A55HT16 sample with (a) intensity distribution (b) volume distribution (c) number distribution fitted with lognormal distribution function (red line). (For interpretation of the references to color in this figure legend, the reader is referred to the web version of this article.)

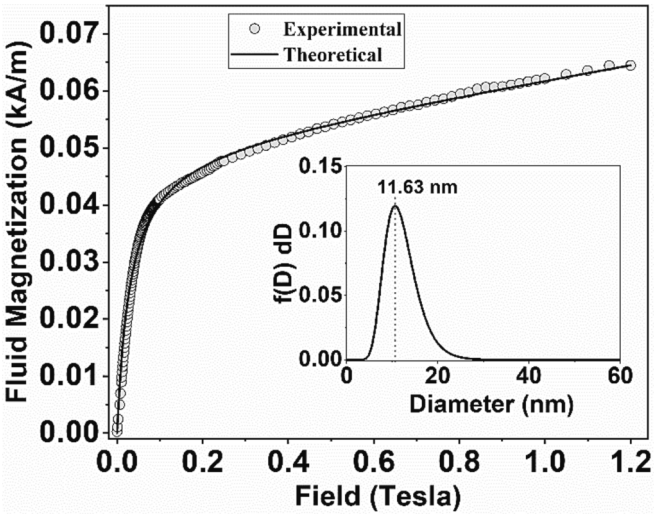

Fig. 5. Magnetic Measurement curve of A55HT16 fluid sample. Inset figure shows the size distribution curve of the fluid.

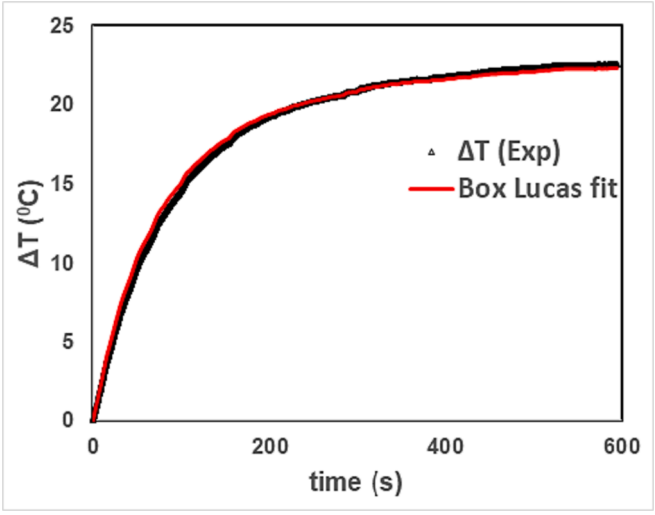

Fig. 6. Temperature rise versus time for a55ht16 sample at 309 kHz frequency.

$\frac{M_s VH}{k_B T}$, the magnetic particle size and size distribution calculated using, $D_{mag} = \left(\frac{6}{\pi V_0}\right)^{1/3}$ and $\sigma_D = \sigma/3$.

$$f(V) \bullet dV = \frac{1}{\sqrt{2\pi}\sigma V} \bullet \exp\left(\frac{-\ln\left(\frac{V}{V_0}\right)^2}{2\sigma^2}\right) \quad (2)$$

Where, V_0 and σ are the mean and standard deviation of volume. The magnetic parameters such as magnetic size of the particles (D_{mag}), size distribution (σ), saturation magnetization (M_S) and paramagnetic susceptibility (χ_{pm}) were measured using a constant domain magnetization of 484 kA/m. The magnetic diameter found for the sample was 11.63 nm and the magnetic size distribution of the magnetic nanoparticles σ = 0.3 was found from the fitting for A55HT16. The obtained saturation magnetization was 0.687 Gauss. The reason for lower magnetization is because of the low concentration (1.8 mg/mL) of the fluid. The paramagnetic susceptibility of the sample found from the fitting was $2x10^{-4}$. The inset of Fig. 5 shows the size distribution curve of the fluid.

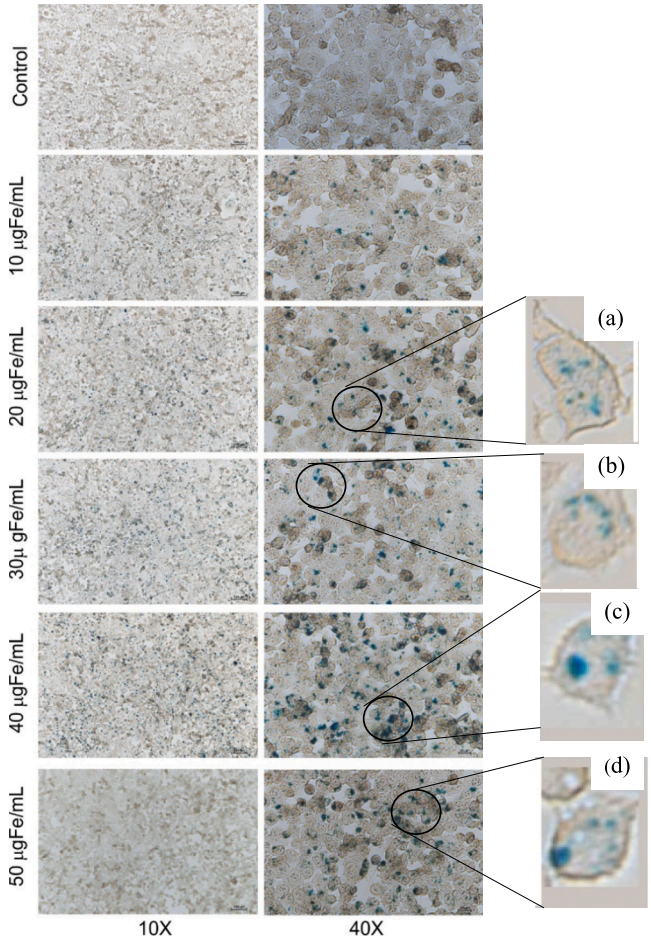

Fig. 7. Images of MDA-MB-231 cells after 18 h of treatment of 10, 20, 30, 40 and 50 μg/mL nanoflowers at 10X and 40X magnifications. The zoom images (a, b, c, d) from these figures confirms the internalization of nanoflowers in the cells.

3.2. Nanoflowers heating potential and SAR calculation

The concentration of magnetic nanoflowers used for the experiment was 1.8 mg/mL. In terms of the experimental estimation, it depends on the rise in temperature of magnetic fluid as a function of time under the constant field and frequency. The initial rate of the temperature rise and the saturation temperature can be used to calculate the specific absorption rate (SAR) using the Box-Lucas fit [26]. The hyperthermic response data was fitted using the Box-Lucas model Eq. (3) given by,

$$\Delta T(t) = A\left(1 - e^{-Bt}\right) \quad (3)$$

Where, ΔT (t) is a rise in temperature with respect to time t, A is the saturation temperature and B is the heating rate. The Fig. 6 shows the rise in temperature with respect to time curves for all the samples fitted with the Box-Lucas equation (solid line). The SAR of the magnetic fluid from the heating curve was calculated using the SAR formula which is shown in Eq. (4).

$$SAR = C_p \bullet \frac{\Delta T}{\Delta t} \bullet \frac{1}{\varphi_{magnetic}} \quad (4)$$

Where, C_p is the combined value of the specific heat capacity of a cluster, $C_{p(cluster)}$, and carrier liquid $C_{p(carrier)}$, with its appropriate mass proportion calculated as $C_{p(fluid)} = m_{cluster} \bullet C_{p(cluster)} + m_{carrier} \bullet C_{p(carrier)}$. Here, $m_{cluster}$ and $m_{carrier}$ defines the weight fraction of cluster and carrier, respectively. In the experiment, the $m_{particles}$ is 0.0018 g and the $m_{carrier}$ is

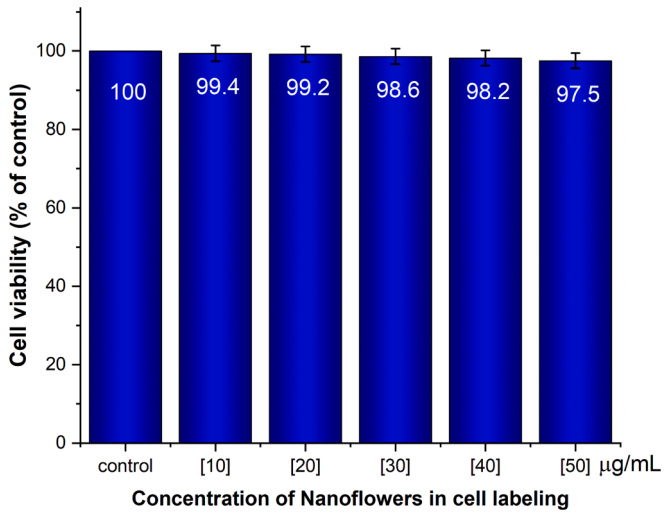

Fig. 8. Evaluation of cell viability by bioluminescence after labeling MDA-MB-231 with nanoflowers.

0.9982 g. $\frac{\Delta T}{\Delta t}$ is the slope of the rise in temperature versus time graph and $\varphi_{magnetic}$ is the weight fraction of magnetic particles. The specific heat capacity of the cluster and carrier (water) was taken as 0.67 and 4.187 $Jg^{-1}K^{-1}$, respectively. The magnetic fraction is determined by dividing the mass of magnetic ion content by the total mass of $Mn_{0.5}Zn_{0.5}Fe_2O_4$. The heating response of the nanoflower suspension is shown in Fig. 6. The value of SAR is calculated from the fitted parameter, which comes out to be 4416.54 W/g_{mag}.

Ganesan et al. [19] has reported 80.5 W/g SAR for iron oxide nanoflowers of 640 nm at 31.6 kA/m of magnetic field and 126 kHz frequency. Similarly, Jamir et al. [20] have reported the maximum of 233.28 W/g of SAR obtained in 1 mg/mL concentration in dextran coated nanoflowers at 336 kHz frequency and 14.92 kA/m magnetic field. The synthesis of different sized nanoflowers from 25 nm to 300 nm was synthesized by Jeong et al. [21] and the heating response of all the samples determined at frequency of 500 kHz, a magnetic field of 37.4 kA/m and concentration of 1 mg/mL. The result of MFH shows that the maximum SAR of 1264 W/g_{Fe} found in the 25 nm sample, although the field and frequency used for measurement was higher than that was used for our study, the heating response of the magnetic fluid is smaller than the present study result. The higher response in our study may be due to (i) smaller cluster size and (ii) a porous structure of cluster where the particles inside the cluster have freedom to move and align in the field direction, helping to respond faster than the other dense clusters.

3.3. Evaluation of nanoflowers internalization in MDA-MB-231 cells

To study the internalization of nanoflowers in MDA-MB-231 cells, the cells were treated with five concentrations (10, 20, 30, 40 and 50 µg/mL) of nanoflowers for a period of 18 h and then Prussian blue staining protocol was used to capture the internalization of the particles. Fig. 7 shows the microscopic images of the cells before and after the treatment of nanoflowers with the cells at 10X and 40X magnifications. It is seen that the cell internalization increases as the concentration of nanoflowers increases (from top to bottom of Fig. 7) and for 40 µg/mL the maximum internalization is seen. The zoom images (a, b, c, d) from these figures confirm the internalization of nanoflowers in the cells. Previous studies [27] have already estimated internalization of similar magnetic nanoparticles in MDA-MB-231 cells. Furthermore, we have observed the formation of aggregates and presence of vacuoles in the cytoplasm, similar to those observed in this analysis [28].

3.4. Cell viability test by bioluminescence technique

The literature has already reported works that used magnetic hyperthermia as a therapeutic approach. In general, the analysis was based on tests such as MTT. Here we demonstrated cell viability through molecular imaging. In Fig. 8 shows the cell viability of nanoflowers on MDA-MB-231 cells tested by Bioluminescence technique using a concentration of particles from 10 to 50 µgFe/mL. It is found that this concentration is a safer concentration and almost 97.5% of cells remain live even after the treatment of these nanoflowers. The literature reports

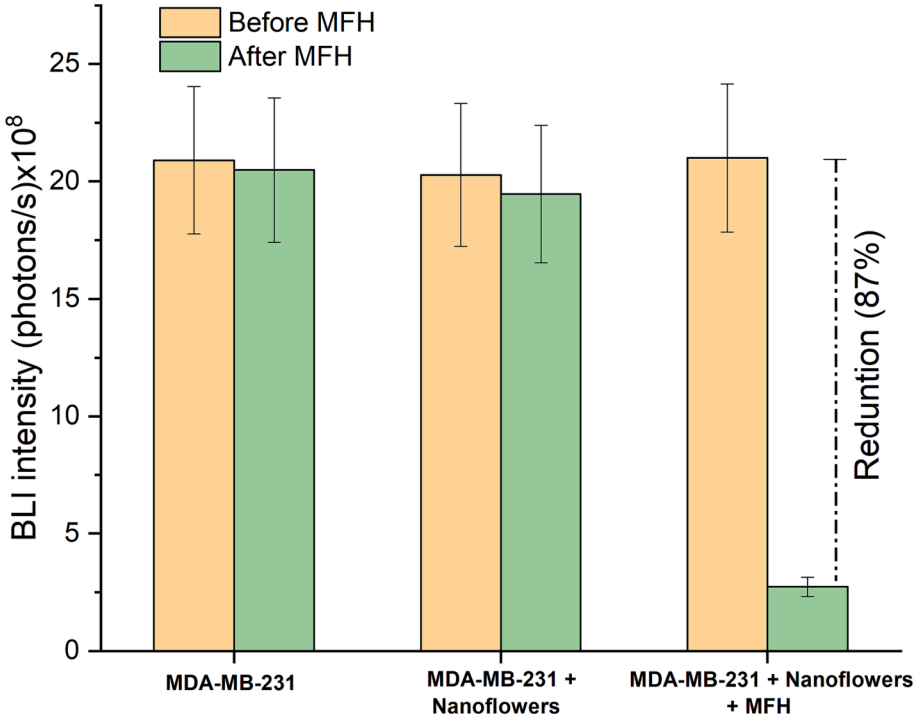

Fig. 9. Bioluminescence intensity (BLI intensity) for three experimental group of samples.

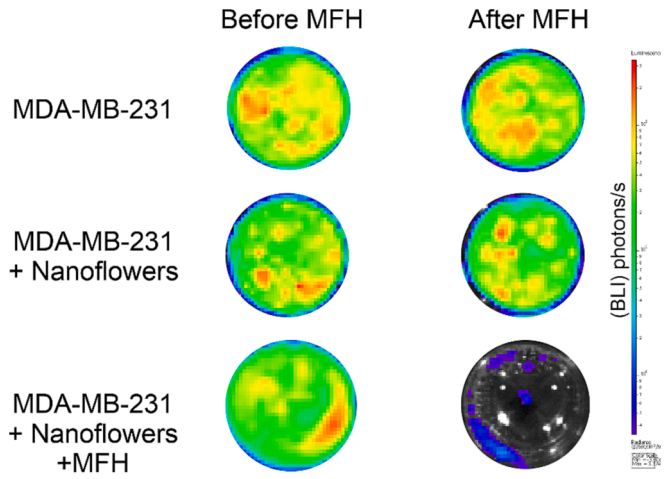

Fig. 10. Bioluminescence intensity images of the experimental groups of magnetic fluid hyperthermia therapy.

Table 1
Bioluminescence intensity in the experimental groups of magnetic fluid hyperthermia therapy.

Conditions	Intensity before MFH (Photons/s)	Intensity after MFH (Photons/s)
MDA-MB-231	2.09×10^9	2.05×10^9
MDA-MB-231 + nanoflowers	2.03×10^9	1.95×10^9
MDA-MB-231 + nanoflowers + MFH	2.10×10^9	2.73×10^8

similar values for other tumor types and some studies have even evaluated higher concentrations in order to determine the potentially cytotoxic concentration [29].

3.5. *In vitro evaluation of magnetic fluid hyperthermia therapy on MDA-MB-231 breast cancer cells*

The *in vitro* MFH therapy was evaluated on the control cells, cells treated with nanoflowers but no hyperthermia treatment and the cells with nanoflowers and MFH treatment. The same is labelled as MDA-MB-231, MDA-MB-231 + nanoflowers and MDA-MB-231 + nanoflowers + MFH in Fig. 9. The MFH parameters were fixed at a magnetic field of 300 Gauss and a frequency of 309 kHz during the treatment. The MFH (23.87 kA/m; 309 kHz) session was maintained for a period of 40 min and during this session a constant temperature of 317 K was observed. It is seen that MFH in cell + nanoflowers + MFH reduces the cell viability up to 87%. This is a very good indication that has been seen using the nanoflowers as compared to other magnetic nanoparticles. Within 40 min duration of MFH, the nanoflowers are capable of destroying almost 87% of cells in a single session..For the similar composition of nanoparticles, it requires either a high concentration and high treatment duration or multiple session hyperthermia to get similar results [30,31].

The bioluminescence evaluation was performed before and after the magneto hyperthermia process, similar to that performed in the above section of cell viability. Fig. 10 shows the image of the same for all three experimental cell groups. The intensity values for the three experimental groups are mentioned in Table 1. The images show the effect of nanoflowers and MFH on cells + nanoflowers which resulted into the black color. These results complement the *in vitro* MFH results on the cell viability as seen from Fig. 9. Furthermore, these results were correlated with the literature, and in fact MFH showed an effect on MDA-MB-231 tumor cells, but also on other types of cells/tumors, such as MCF7 [30] or PaCa-2 and PANC-1, pancreatic ductal adenocarcinoma [29].

4. Conclusion

The present report concludes the synthesis of stable magnetic nanoflowers based magnetic fluid using a hydrothermal route for the magnetic fluid hyperthermia. The size of nanoflowers determined by the TEM size is around 106.8 nm with a standard deviation of 0.1 nm. Within a single cluster there are 19.25 nm size particles with polydispersity of 0.07. The size of particles matches with the crystallite size from XRD and the magnetic size from magnetic measurement. Magnetic nanoflowers dispersion is found to be very effective for magnetic fluid hyperthermia on breast cancer cells. The fluid is non-toxic and effectively kills cancerous cells within 30 min of treatment. The induction heating of 40 min on MDA-MB-231 cells shows almost 87% killing of cancerous cells, which shows high effectiveness of the sample synthesized.

Declaration of Competing Interest

The authors declare that they have no known competing financial interests or personal relationships that could have appeared to influence the work reported in this paper.

Data availability

Data will be made available on request.

Acknowledgements

HP thank Government of Gujarat for financial support under SHODH scheme (student Reference no. 202001300004). KP thank GOI, for providing grant no. SERB/CRG/2021/001587. KP also thank FAPESP (grant 2022/04512-5) for providing financial support to carry out the experimental study at USP, Brazil.

References

[1] H.P. Kok, P. Wust, P.R. Stauffer, F. Bardati, G.C. Van Rhoon, J. Crezee, Current state of the art of regional hyperthermia treatment planning: a review, Radiat. Oncol. (2015) 1–14, https://doi.org/10.1186/s13014-015-0503-8.
[2] A. Jordan, et al., Effects of Magnetic Fluid Hyperthermia (MFH) on C3H mammary carcinoma in vivo, Int. J. Hyperth. 13 (6) (1997) 587–605, https://doi.org/10.3109/02656739709023559.
[3] A. Jordan, et al., Inductive heating of ferrimagnetic particles and magnetic fluids: physical evaluation of their potential for hyperthermia, Int. J. Hyperth. ISSN 25 (7) (2009) 499–511, https://doi.org/10.3109/02656730903287790.
[4] R.E. Rosensweig, Heating magnetic fluid with alternating magnetic field, J. Magn. Magn. Mater. 252 (2002) 370–374, https://doi.org/10.1016/S0304-8853(02)00706-0.
[5] U.S. Patil, S. Adireddy, A. Jaiswal, S. Mandava, B.R. Lee, In Vitro / In Vivo Toxicity Evaluation and Quantification of Iron Oxide Nanoparticles (2015), https://doi.org/10.3390/ijms161024417.
[6] B. Laffon, N.F. Bertólez, C. Costa, F. Brandão, J.P. Teixeira, E. Pásaro, V. Valdiglesias, Cellular and molecular toxicity of iron oxide nanoparticles, Adv. Exp. Med. Biol. 1048 (2018) 199–213, https://doi.org/10.1007/978-3-319-72041-8_12.
[7] B. Hildebrandt, et al., The cellular and molecular basis of hyperthermia, Crit. Rev. Oncol. Hematol. 43 (2002) 33–56, https://doi.org/10.1016/S1040-8428(01)00179-2.
[8] G.N.A. Rego, et al., Therapeutic Efficiency of Multiple Applications of Magnetic Hyperthermia Technique in Glioblastoma Using Aminosilane Coated Iron Oxide Nanoparticles. In Vitro and In Vivo Study, Int. J. Mol. Sci. 21 (3) (2020) 958, https://doi.org/10.3390/ijms21030958.
[9] D. Rahban, M. Doostan, A. Salimi, Cancer Therapy; Prospects for Application of Nanoparticles for Magnetic-Based Hyperthermia, Cancer Invest. 38 (8–9) (2020) 507–521, https://doi.org/10.1080/07357907.2020.1817482.
[10] Z. Farzanegan, M. Tahmasbi, Evaluating the applications and effectiveness of magnetic nanoparticle-based hyperthermia for cancer treatment: A systematic review, Appl. Radiat. Isot. 198 (November 2022) (2023) 110873, https://doi.org/10.1016/j.apradiso.2023.110873.
[11] A.T. Apostolov, I.N. Apostolova, J.M. Wesselinowa, Ferrimagnetic nanoparticles for self-controlled magnetic hyperthermia, Eur. Phys. J. B 86 (483) (2013) 1–10, https://doi.org/10.1140/epjb/e2013-40791-9.
[12] M. Veverka, et al., Synthesis and magnetic properties of Co 1 À x Zn x Fe 2 O 4 + g nanoparticles as materials for magnetic fluid hyperthermia, J. Magn. Magn. Mater. 322 (2010) 2386–2389, https://doi.org/10.1016/j.jmmm.2010.02.042.

[13] K. Parekh, R.V. Upadhyay, Magnetization dynamics in rare earth Gd3+ doped Mn0.5Zn0.5Fe2O4 magnetic fluid: Electron spin resonance study, J. Magn. Reson. 225 (2012) 46–51, https://doi.org/10.1016/j.jmr.2012.10.001.
[14] R.V. Upadhyay, K. Parekh, L. Belova, K.V. Rao, Low-field DC-magnetization study of Ho 3 + -doped Mn – Zn ferrite ferrofluid, J. Magn. Magn. Mater. 311 (2007) 106–110, https://doi.org/10.1016/j.jmmm.2006.10.1197.
[15] H. Das, et al., Influence of crystallite size on the magnetic and heat generation properties of La0.77Sr0.23MnO3 nanoparticles for hyperthermia applications, J. Phys. Chem. Solid 112 (2017) 179–184, https://doi.org/10.1016/j.jpcs.2017.09.030.
[16] R. Desai, V. Davariya, K. Parekh, R.V. Upadhyay, Structural and magnetic properties of size-controlled Mn 0.5Zn0.5Fe2O4 nanoparticles and magnetic fluids, Pramana - J. Phys. 73 (4) (2009) 765–780, https://doi.org/10.1007/s12043-009-0144-2.
[17] K. Parekh, H. Parmar, V. Sharma, Effect of Me 2 + / OH − ratio in the formation of Mn 0. 5 Zn 0. 5 Fe 2 O 4 nanoparticles of different sizes and shapes in association with thermomagnetic property, Pramana 4 (2020), https://doi.org/10.1007/s12043-020-01945-6.
[18] R.V. Upadhyay, R.V. Mehta, K. Parekh, D. Srinivas, R.P. Pant, Gd-substituted ferrite ferrofluid: A possible candidate to enhance pyromagnetic coefficient, J. Magn. Magn. Mater. 201 (1–3) (1999) 129–132, https://doi.org/10.1016/S0304-8853(99)00034-7.
[19] V. Ganesan, B.B. Lahiri, C. Louis, J. Philip, S.P. Damodaran, Size-controlled synthesis of superparamagnetic magnetite nanoclusters for heat generation in an alternating magnetic field, J. Mol. Liq. 281 (2019) 315–323, https://doi.org/10.1016/j.molliq.2019.02.095.
[20] M. Jamir, R. Islam, L.M. Pandey, J.P. Borah, Effect of surface functionalization on the heating efficiency of magnetite nanoclusters for hyperthermia application, J. Alloy. Compd. 854 (2021), 157248, https://doi.org/10.1016/j.jallcom.2020.157248.
[21] M. Jeong, S. Lee, D. Y. Song, S. Kang, T. Shin, J. Choi, Hyperthermia Effect of Nanoclusters Governed by Interparticle Crystalline Structures, 2021, doi: 10.1021/acsomega.1c04632.
[22] H. Rodrigues, et al., Triple-modal imaging of stem-cells labeled with multimodal nanoparticles, applied in a stroke model, World J. Stem Cells 11 (2) (2019) 100–124, https://doi.org/10.4252/wjsc.v11.i2.100.
[23] M.P. Nucci, et al., Optimization of Multimodal Nanoparticles Internalization Process in Mesenchymal Stem Cells for Cell Therapy Studies, Pharmaceutics 14 (6) (2022) 1–23, https://doi.org/10.3390/pharmaceutics14061249.
[24] K. Parekh, R.V. Upadhyay, L. Belova, K.V. Rao, Ternary monodispersed Mn0.5Zn0.5Fe2O 4 ferrite nanoparticles: Preparation and magnetic characterization, Nanotechnology 17 (24) (2006) 5970–5975, https://doi.org/10.1088/0957-4484/17/24/011.
[25] D. Chen, et al., Size determination of superparamagnetic nanoparticles from magnetization curve Size determination of superparamagnetic nanoparticles from magnetization 083924 (2009) (2014), https://doi.org/10.1063/1.3117512.
[26] R.R. Wildeboer, P. Southern, Q.A. Pankhurst, On the reliable measurement of specific absorption rates and intrinsic loss parameters in magnetic hyperthermia materials, J. Phys. D Appl. Phys. 47 (49) (2014) pp, https://doi.org/10.1088/0022-3727/47/49/495003.
[27] Y. Cai, et al., Enhanced magnetic resonance imaging and staining of cancer cells using ferrimagnetic H-ferritin nanoparticles with increasing core size, Int. J. Nanomed. 10 (2015) 2619–2634, https://doi.org/10.2147/IJN.S80025.
[28] E. Catalano, C. Enrico, Superparamagnetic iron oxide nanoparticles conjugated with doxorubicin for targeting breast cancer, 2019. doi: 10.48550/arXiv.1911.05378.
[29] J. Palzer, B. Mues, R. Goerg, T. Cramer, T. Schmitz-rode, U.P. Neumann, Magnetic Fluid Hyperthermia as Treatment Option for Pancreatic Cancer Cells and Pancreatic Cancer Organoids, Int. J. Nanomed. 16 (2021) 2965–2981, https://doi.org/10.2147/IJN.S288379.
[30] A. Bhardwaj, K. Parekh, N. Jain, In vitro hyperthermic effect of magnetic fluid on cervical and breast cancer cells, Sci. Rep. 10 (1) (2020) 1–13, https://doi.org/10.1038/s41598-020-71552-3.
[31] A. Bhardwaj, N. Jain, K. Parekh, Investigating the effect of outer layer of magnetic particles on cervical cancer cells HeLa by magnetic fluid hyperthermia, Cancer Nanotechnol. (2021) 1–20, https://doi.org/10.1186/s12645-021-00076-w.